



Efficient electrochemiluminescent cyclometalated iridium(III) complexes: Synthesis, photophysical and electrochemiluminescent properties

Chunxiang Li, Juan Lin, Xiaoyan Yang, Jun Wan*

State Key Laboratory Base of Eco-chemical Engineering, College of Chemistry and Molecular Engineering, Qingdao University of Science and Technology, Qingdao 266042, PR China

ARTICLE INFO

Article history:

Received 23 November 2010

Received in revised form

2 March 2011

Accepted 8 March 2011

Keywords:

Cyclometalated Ir complex
Electrochemiluminescence(ECL)
Synthesis

ABSTRACT

A series of new cyclometalated iridium(III) complexes for electrochemiluminescence (ECL) system were synthesized and fully characterized. Using tri-*n*-propylamine (TPA) as an oxidative–reductive co-reactant, their ECL properties were studied in acetonitrile (CH₃CN) and mixed CH₃CN/H₂O (50:50, v/v) solutions, respectively. Meanwhile, the influencing factors of ECL efficiencies, including working electrode, pH, and surfactant were investigated. A remarkable ECL enhancement (up to about 13.5 times), in comparison with the commonly used Ru(bpy)₃²⁺ (2,2'-bipyridyl) ruthenium(II), is observed from Ir(FPP)₂(acac) (where FPP is 2-(4-fluorophenyl)-4-phenylpyridine, acac = acetylacetonate) at Pt disk electrode. At the same time, an increase in ECL efficiency is also observed in surfactant media. This study provided a new method for further improving and tuning the ECL efficiency by designing new iridium complexes with the appropriate cyclometalated or ancillary ligands.

© 2011 Elsevier B.V. All rights reserved.

1. Introduction

Electrogenerated chemiluminescence (ECL) has long been of interest because it provides an important and powerful tool for various applications owing to its simplicity, low cost and high sensitivity. Among the various luminescent materials investigated for ECL study, an important branch is metal complexes, and most of the ECL studies on metal complexes have been focused on Ru(II) complexes due to their relatively high emission quantum yield and long excited-state lifetimes [1–4]. Though Ru(bpy)₃²⁺ (2,2'-bipyridyl) ruthenium(II) and its derivatives have been studied as the important ECL luminophores for decades [1,5–7], much effort has been directed to develop new ECL luminophores to improve the sensitivity.

Recently, the luminescent materials used for OLED (organic light emitting devices) such as Al(III) [8], Pt(II) [9], Os(II) [10], Eu(II) [11], and cyclometalated Ir(III) [12–17] complexes have been studied as new ECL reagents. Among the various transition metal complexes, researchers pay much more attention to the cyclometalated iridium (III) complexes, which are promising materials for ECL studies for their remarkable photoluminescent properties. For example, (pq)₂Ir(acac) (pq = 2-phenylquinoline, acac = acetylacetonate), has an excellent luminescence property with

$\Phi_{em} = 0.1$, and shows intense ECL via the annihilation reaction [17–19]. These properties are due to efficient intersystem crossing between the singlet and triplet excited states of the iridium(III) [20]. The general formula of neutral heteroleptic complexes is [Ir(C^N)₂(X^X)] (X = O, N), where the symbols C^N and X^X represent the cyclometalated and ancillary ligands, respectively. Both the luminescent efficiency and emission wavelength of these species can usually be tuned by the introduction of various cyclometalated and ancillary ligands which can control the relative positions of HOMO and LUMO levels (oxidation potential and reduction potential) [21]. Some recent reports also demonstrate that iridium complexes really have interesting ECL properties, and the possible mechanism has been proposed [22,23]. All these prompted us to design a series of novel cyclometalated and ancillary ligands to find new ECL reagents and to improve the sensitivity of ECL sensors by replacing conventional the Ru(bpy)₃²⁺ complex.

In this work, several neutral *tris*-chelate iridium(III) complexes, Ir(FPP)₂(acac), Ir(FBPI)₂(acac), Ir(FBPI)₂(pic), Ir(FBPI)₂(pmp), and Ir(MDX)₂(acac) (FPP = 2-(4-fluorophenyl)-4-phenylpyridine, FBPI = 1-(4-fluorobenzyl)-2-(4-fluorophenyl)-1*H*-benzo[*d*]imidazole, MDX = 2,5-dip-tolyl-1,3,4-oxadiazole, pic = picolinic acid, pmp = 2-((phenylimino) methyl) phenol) (Fig. 1) were prepared and their investigations of the structure, optical, and electrochemical properties are reported. The effects of various factors on the ECL behavior, such as pH, working electrode, the concentration of electrolyte, and surfactant were also examined.

* Corresponding author. Tel./fax: +86 532 84022750.

E-mail address: moze0802@yahoo.com.cn (J. Wan).

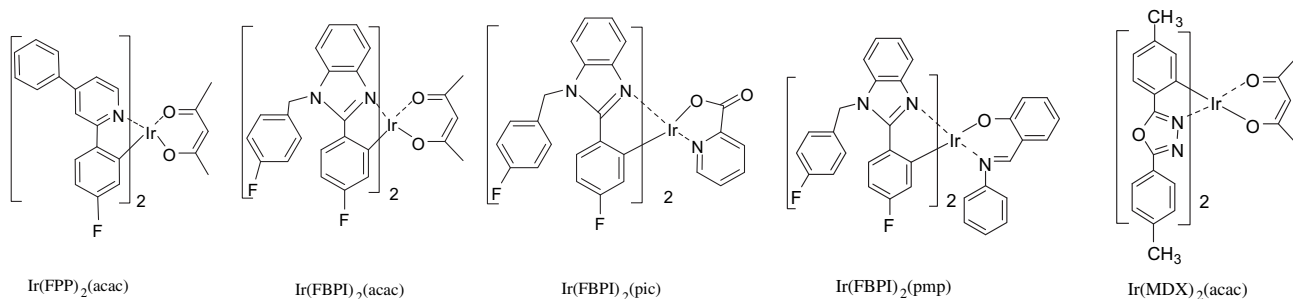
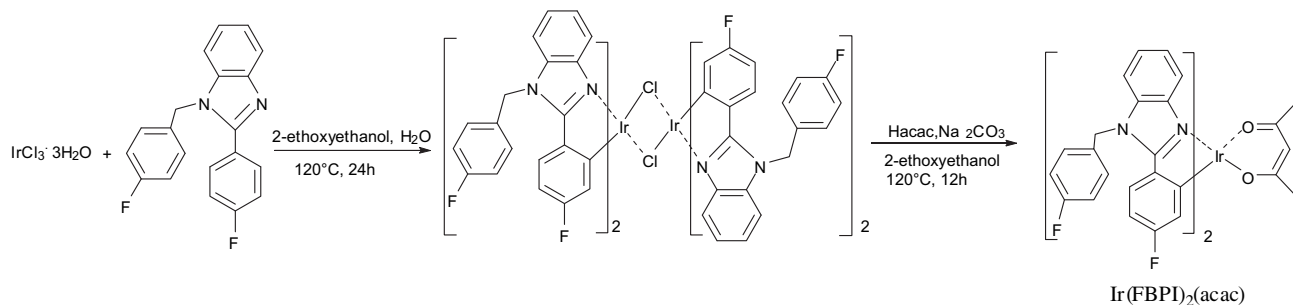


Fig. 1. Structures of iridium complexes used in ECL study.



Scheme 1. Synthesis of the Ir(FBPI)₂(acac) complex.

2. Results and discussion

2.1. Synthesis and characterization of iridium complexes

The iridium complexes are prepared by a conventional two-step sequence as shown in Scheme 1, taking Ir(FBPI)₂(acac) for example. Heating the cyclometalated ligand with IrCl₃·3H₂O in solution (ethoxyethanol: H₂O = 3:1 (V)) gives a dichloro-bridged ortho-metalated dimers. Then, treatment of the dimers with an appropriate ancillary ligands and Na₂CO₃ in acetyl acetone solution gives the corresponding cyclometalated iridium complexes with the overall yield of about 28–38%. The obtained complexes were

characterized by ¹H NMR, elemental analysis, IR and mass spectroscopy. High-purity samples of complexes for electrochemical and luminescence investigations were obtained by crystallization. Single crystals of complexes Ir(FPP)₂(acac) and Ir(MDX)₂(acac) were grown from CH₂Cl₂ solution and characterized by X-ray crystallography.

The crystallographic data are shown in Table 1, and the selected bond lengths and angles are given in Tables 2 and 3, respectively. The crystal structures are shown in Fig. 2. The complex, Ir(FPP)₂(acac), crystallizes in the monoclinic unit cell with space group C2/c, while complex Ir(MDX)₂(acac) in triclinic with *P*-1. In the two structures, iridium (III) adopts a distorted octahedral geometry, with the C and N atoms belonging to cyclometalated ligands in *cis* and *trans* configurations, respectively. The Ir(FPP)₂(acac) molecule lies in a two-fold axis crystallographically, which accounts for an equivalent pattern in the proton NMR peaks of the two chelated ligands. The Ir–C bond lengths (1.954–2.013 Å) are within the interval observed for the corresponding distance in iridium C[^]N chelates with similar geometry and ligand environments [24].

Table 1
Crystal data and structure refinement for Ir(FPP)₂(acac) and Ir(MDX)₂(acac).

Complex	Ir(FPP) ₂ (acac)	Ir(MDX) ₂ (acac)
Empirical formula	C ₃₉ H ₂₉ N ₂ O ₂ F ₂ Ir	C ₃₇ H ₃₃ N ₄ O ₄ Ir·CH ₂ Cl ₂
Formula weight	787.84	874.82
Crystal system	monoclinic	triclinic
Space group	C2/c	<i>P</i> -1
Unit cell dimensions		
<i>a</i> (Å)	20.445(7)	10.299(3)
<i>b</i> (Å)	10.359(4)	13.330(4)
<i>c</i> (Å)	15.171(5)	14.184(4)
α (deg)	90	92.487(4)
β (deg)	93.626(4)	108.287(3)
γ (deg)	90	98.325(4)
Volume, Å ³	3207(2)	1821.2(9)
<i>Z</i>	4	2
<i>D</i> _{calc} , g/cm ³	1.632	1.595
<i>F</i> (000)	1552	868
Abs coeff, mm ⁻¹	4.213	3.857
Crystal Size, mm	0.24 × 0.26 × 0.32	0.22 × 0.24 × 0.28
θ range	2.0–26.0	2.1–26.0
Independent reflections	3131 [<i>R</i> (int) = 0.031]	7036 [<i>R</i> (int) = 0.032]
Data/restraint/parameters	3131/0/198	7036/0/448
Goodness-of-fit on <i>F</i> ²	1.062	1.008
<i>R</i>	0.0439	0.0580
<i>wR</i>	0.0903	0.1234

Table 2
Selected bond distance (Å) and angle (°) for Ir(FPP)₂(acac).

Bond distance (Å)			
Ir(1)–C(1)	1.954(7)	N(1)–C(7)	1.330(8)
Ir(1)–N(1)	2.062(4)	N(1)–C(11)	1.360(8)
Ir(1)–O(1)	2.110(5)		
Bond angle (°)			
O(1)–Ir(1)–C(1)	91.4(2)	O(1)–Ir(1)–O(1A)	88.13(18)
O(1)–Ir(1)–N(1A)	94.59(18)	O(1)–Ir(1)–C(1A)	174.5(2)
N(1)–Ir(1)–C(1)	80.0(2)	O(1A)–Ir(1)–N(1)	94.59(18)
N(1)–Ir(1)–N(1A)	171.7(2)	N(1)–Ir(1)–C(1A)	94.1(2)
O(1A)–Ir(1)–C(1)	174.5(2)	N(1A)–Ir(1)–C(1)	94.1(2)
N(1A)–Ir(1)–C(1)	94.1(2)	C(1)–Ir(1)–C(1A)	89.6(3)
O(1A)–Ir(1)–N(1A)	91.39(18)	O(1A)–Ir(1)–C(1A)	91.4(2)
N(1A)–Ir(1)–C(1A)	80.0(2)	Ir(1)–O(1)–C(19)	125.5(5)

Table 3
Selected bond distance (Å) and angle (°) for Ir(MDX)₂(acac).

Bond distance (Å)			
Ir(1)–O(3)	2.127(5)	Ir(1)–C(1)	2.013(7)
Ir(1)–O(4)	2.126(5)	Ir(1)–C(17)	2.008(8)
Ir(1)–N(1)	2.029(7)	N(1)–N(2)	1.392(10)
Ir(1)–N(3)	2.030(7)	N(3)–N(4)	1.393(10)
Bond angle (°)			
O(3)–Ir(1)–O(4)	89.1(2)	N(1)–Ir(1)–C(1)	79.6(3)
O(3)–Ir(1)–N(1)	98.8(2)	N(1)–Ir(1)–C(17)	93.8(3)
O(3)–Ir(1)–N(3)	89.6(3)	N(3)–Ir(1)–C(1)	91.9(3)
O(3)–Ir(1)–C(17)	87.0(3)	N(3)–Ir(1)–C(17)	79.8(3)
O(4)–Ir(1)–N(3)	98.5(2)	C(1)–Ir(1)–C(17)	91.8(3)
O(4)–Ir(1)–C(1)	92.1(3)	N(1)–Ir(1)–N(3)	169.2(3)
O(4)–Ir(1)–C(17)	175.7(3)	Ir(1)–N(1)–N(2)	137.9(5)

2.2. Absorption and fluorescent emission

The absorption spectra and phosphorescence emission spectra of all complexes were recorded at room temperature in CH₃CN solution and are reported in Fig. 3. The results are gathered in Table 4. The UV region displays the ligand-centered (LC) $\pi \rightarrow \pi^*$ transitions as the most intense absorption bands, for each species. The shoulders appearing in the range of 330–453 nm are likely due to charge-transfer (CT) transitions, with their nature being both spin-allowed ¹MLCT and spin-forbidden ³MLCT according to the previous reports and the calculations of Hay [25]. On irradiation with appropriate wavelengths, all of the iridium complexes show strong photoluminescence in CH₃CN, while falling in green to red region. It is attributed to the presence of an excited-state resulting from the mixing of comparable percentages of ³LC and ³MLCT states, which is in agreement with Bandini's work concerning analogous iridium complexes [26]. Strong spin-orbit coupling of central metal atoms facilitates the spin-forbidden ³MLCT transitions of the metal complexes. The photoluminescence efficiencies (Φ_{em}) for these iridium complexes are substantially greater than Ru(bpy)₃²⁺ ($\Phi_{em} \sim 0.042$), ranging from 0.125, as in the case of Ir(MDX)₂(acac), to 0.268 for Ir(FBPI)₂(pmp). This intense phosphorescence of complexes is readily visible in the daylight using UV light.

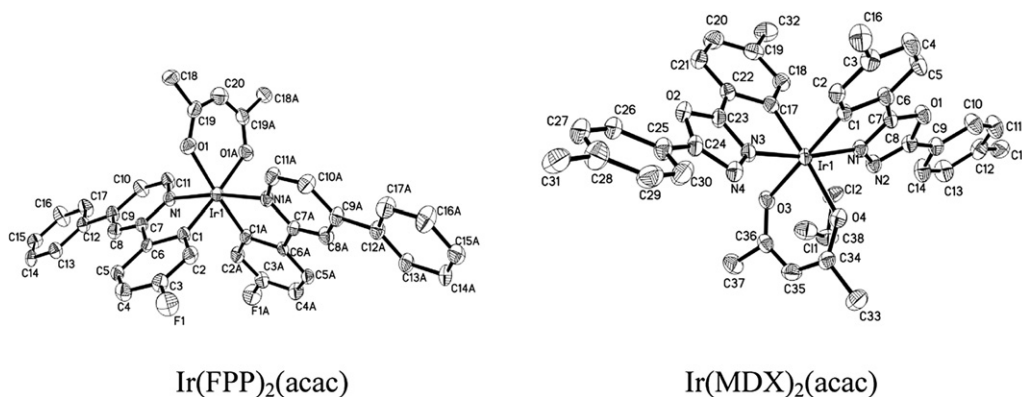
2.3. Electrochemistry

The electrochemical properties of these complexes were employed in CH₃CN solution by cyclic voltammetry at room temperature, in which the *i*–*V* response can provide information on the kinetics of the electron-transfer reaction and thermodynamics of the electrode–electrolyte interface. The potentials of oxidation

process are collected in Table 4. In the region of positive potential, all of the complexes exhibit a single one-electron-transfer reversible process. As an example, the CV curve of positive potential for Ir(MDX)₂(acac) is shown in Fig. 4, the observed oxidative wave ($E_{1/2} = 0.71$ V vs Fc/Fc⁺) is assigned to Ir(MDX)₂(acac)^{0/+1}. The redox chemistry shows that the peak current ratio (i_a/i_c) and peak separation (ΔE_{pp}) is 0.90 and 0.08 V, respectively, indicating a reversible one-electron-transfer system. As previously reported [27–29], the oxidation of this species can be mainly attributed to the metal center, with a substantial contribution from the ligands, however, the reduction process are mainly localized on the ligands, with only a partial contribution from the metal center.

2.4. Electrochemiluminescence

The ECL performances for the synthesized complexes were studied with TPA as an “oxidative–reductive” co-reactant in CH₃CN. The ECL spectra of these complexes are obtained in CH₃CN and show some differences compared to the luminescence, being slightly broader in shape (Figs. 3 and 5), with λ_{max} approximately shifted 10 nm, respectively, indicating that the ECL emission is due to the MLCT transitions [13,17]. This difference is probably due to the concentration variation and the lower resolution of the ECL instrument. To learn more about the new ECL, various factors influencing ECL such as the concentration of co-reactant and supporting electrolyte, and working electrode were studied in CH₃CN. The results show that the optimum conditions for the system are: working electrode is Pt disk electrode; the concentrations of TPA and Bu₄NPF₆ are 0.025 and 0.05 M, respectively. Extremely high ECL efficiencies are obtained with the iridium complexes as emitter except Ir(FBPI)₂(pmp). Under the same concentration of emitter, Ir(FPP)₂(acac) and Ir(MDX)₂(acac) show 13.5 and 11.5 times, respectively, compared to Ru(bpy)₃²⁺/TPA system. According to the references [17,22], it is believed that the complexes have suitable oxidation potential. On one hand, it should be positive enough for an efficient generation of TPA^{•+} (potential of TPA/TPA^{•+} is 0.80 V vs Ag/AgCl) [30]. On the other hand, they have relatively low oxidation potential to be easily oxidized to Ir complex positive ions. And the relative stability of metal complexes during the ECL measurements can generate these high ECL efficiencies. The Φ_{ECL} of Ir(MDX)₂(acac) is more 40 times higher than that of Ir(ppy)₃ (ppy = 2-phenylpyridine) reported by Richter [13]. Lee reported that (pq)₂Ir(acac) and (pq)₂Ir(tmd) (pq = 2-phenylquinoline anion, tmd = 2,2',6,6'-tetramethylhepta-3,5-dione anion) gave very high ECL compared to Ir(MDX)₂(acac) (6 and 4 times for (pq)₂Ir(acac) and (pq)₂Ir(tmd), respectively) [17]. Though synthesized Ir complexes in this paper can not give the highest efficiency, the results can provide extensive

**Fig. 2.** ORTEP diagram of Ir(FPP)₂(acac) and Ir(MDX)₂(acac).

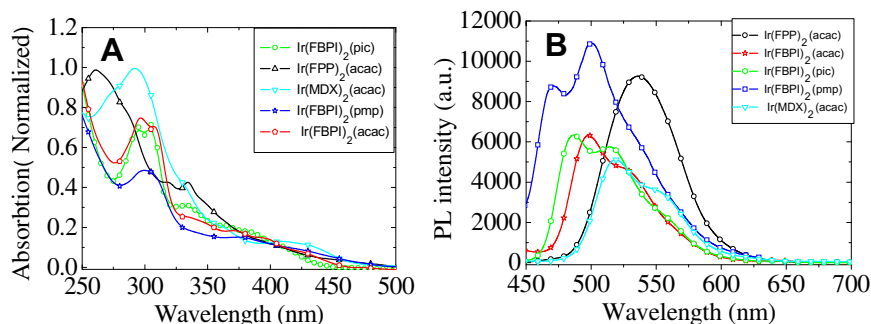


Fig. 3. Absorption and Photoluminescence spectra of 10 M Iridium complexes in CH_3CN solution at 25°C ; Excitation wavelengths are as followed: $\text{Ir}(\text{FPP})_2(\text{acac})$: 340 nm; $\text{Ir}(\text{FBPI})_2(\text{acac})$: 320 nm; $\text{Ir}(\text{FBPI})_2(\text{pic})$: 325 nm; $\text{Ir}(\text{MDX})_2(\text{acac})$: 310 nm; $\text{Ir}(\text{FBPI})_2(\text{pmp})$: 330 nm.

information for future ECL studies. The low Efficiency of $\text{Ir}(\text{FBPI})_2(\text{pmp})$, $\text{Ir}(\text{FBPI})_2(\text{pic})$ and $\text{Ir}(\text{FBPI})_2(\text{acac})$ is mainly contributed to the poor solubility.

To use these types of compounds in immunoassays and DNA analysis, the ECL performances in mixed $\text{CH}_3\text{CN}/\text{H}_2\text{O}$ (50:50, v/v) and aqueous (0.1 M KH_2PO_4) solutions were also studied, respectively. Appreciable decrease of the ECL intensity in mixed solution for these complexes can be observed (summarized in Table 4), which may be due to the poor solubility and unstability of complexes in presence of H_2O , especially for $\text{Ir}(\text{FBPI})_2(\text{pic})$ and $\text{Ir}(\text{FBPI})_2(\text{pmp})$. The surfactant Triton X-100 (poly-(ethylene glycol) *tert*-octylphenyl ether) was adopted for $\text{Ir}(\text{FPP})_2(\text{acac})$ and $\text{Ir}(\text{MDX})_2(\text{acac})$ system in order to regulate solubility of complexes and improve ECL efficiency in mixed solution. Fig. 6 illustrates the relationship between surfactant concentration and ECL intensity for $\text{Ir}(\text{FPP})_2(\text{acac})$ and $\text{Ir}(\text{MDX})_2(\text{acac})$. The ECL intensity is increased significantly in presence of surfactant, especially for $\text{Ir}(\text{MDX})_2(\text{acac})$, which is reached up to approximately 8 times stronger than that of no surfactant addition. It is believed that adsorption of Triton X-100 renders the electrode more hydrophobic, facilitating TPA and luminophore oxidation and leading to higher ECL intensities, according to Richter's point [14]. This provides a promising method to obtain high efficiency in mixed solution.

The ECL emission is also pH dependent in 50:50 (v/v) $\text{CH}_3\text{CN}/\text{H}_2\text{O}$ solutions, and maximum intensities observed were pH ~ 8 for $\text{Ir}(\text{MDX})_2(\text{acac})$ and pH ~ 9 (The pH of buffer solutions was adjusted by 0.1 M KH_2PO_4 , 0.1 M K_2HPO_4 and 6 M NaOH) for $\text{Ir}(\text{FPP})_2(\text{acac})$, respectively (Fig. 7). Similar trends are observed for $\text{Ru}(\text{bpy})_3^{2+}$ using TPA as a co-reactant. This is important for potential applications since the pH of environmental and biological systems is ~ 7.4 and would require less sample preparation prior to analysis. It also improves that both ruthenium- and iridium-based complexes can be presented in the same sample solution for multi-analyt ECL determination.

Table 4
Optical and electrochemical properties of iridium complexes.

Complex	PL		Electrochemistry (V vs Fc/Fc^+)			
	$\lambda_{\text{max}}/\text{nm}$	Φ_{em}^a	$E_{1/2}(\text{ox})(\text{V})^b$	$\lambda_{\text{max}}/\text{nm}^b$	Rel Φ_{ECL}^c	
					CH_3CN	$\text{CH}_3\text{CN}/\text{H}_2\text{O}$ (50:50)
$\text{Ir}(\text{FPP})_2(\text{acac})$	535	0.23	0.35	545	13.5	1.51
$\text{Ir}(\text{FBPI})_2(\text{acac})$	497, 529	0.15	0.28	500	2.5	0.107
$\text{Ir}(\text{FBPI})_2(\text{pic})$	486, 514	0.16	0.46	490	2	0.088
$\text{Ir}(\text{FBPI})_2(\text{pmp})$	470, 524	0.27	0.45	510	0.05	0.081
$\text{Ir}(\text{MDX})_2(\text{acac})$	518	0.13	0.67	520	11.5	6.53

^a Values obtained in thoroughly degassed CH_3CN solution using $\text{Ru}(\text{bpy})_3^{2+}$ ($\Phi_{\text{em}} = 0.042$) as a standard.

^b Values obtained in CH_3CN .

^c Relative ECL efficiency with respect to $\text{Ru}(\text{bpy})_3^{2+}$ ($\Phi_{\text{ECL}} = 1$).

3. Conclusions

A series of new air-stable cyclometalated iridium(III) complexes were prepared and fully characterized by studying their crystallographic, luminescence, and electrochemical properties. The ECL behavior of the synthesized $\text{Ir}(\text{III})$ complexes and specific influences of ECL efficiency have been investigated. Extremely efficient ECLs, some of which even approached $13.5\times$ higher than that of $\text{Ru}(\text{bpy})_3^{2+}$, have been observed with TPA as a co-reactant at reasonable voltage and pH levels. Additionally, ECL efficiency is increased in the presence of surfactant. The synthesized $\text{Ir}(\text{III})$ chelates emit over a range of wavelengths, from blue to green, which allow designing efficient multicolor ECL systems to achieve the analysis of multiple analytes in the same solution. The fact that the electrochemical and ECL behavior of $\text{Ir}(\text{III})$ complexes are very similar to those of $\text{Ru}(\text{bpy})_3^{2+}$ indicates that our highly efficient $\text{Ir}(\text{III})$ complexes can be used in many interesting applications by replacing conventional the $\text{Ru}(\text{bpy})_3^{2+}$ complex. It is expected that the sensitivity of ECL sensors can be increased more than 10 times. Further study about the application of the $\text{Ir}(\text{III})$ complexes in ECL sensors is in progress.

4. Experimental sections

4.1. Apparatus

^1H NMR spectra were measured on Bruker ARX-300 (300 MHz) spectrometer, using TMS as internal standard. Mass spectra (MS) were measured on a VG-ZAB-MS spectrometer with electron impact ionization. Elemental analysis was performed on a Perkin-Elmer 240C elemental analyzer. The UV-Vis spectra were recorded on VARIAN Cary 5000 spectrometer. Phosphorescence spectra were recorded by Perkin-Elmer LS 50B luminescence

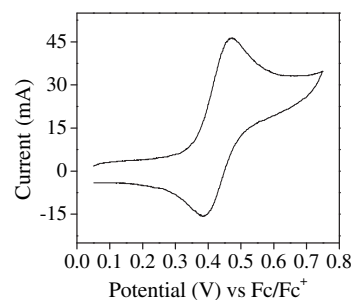


Fig. 4. Cyclic voltammogram (record at Pt electrode with scan rate $V_p = 100 \text{ mV s}^{-1}$) of 0.1 mM $\text{Ir}(\text{MDX})_2(\text{acac})$ in CH_3CN solutions containing 0.1 M Bu_4NPF_6 as supporting electrolyte. Potential scale according to the internal Fc/Fc^+ reference redox system.

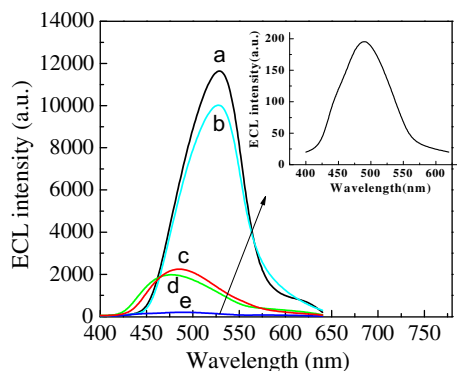


Fig. 5. ECL spectra of iridium complexes of 10 μM in CH_3CN solution: Bu_4NPF_6 as supporting electrolyte, TPA as oxidative–reductive co-reactant.

spectrophotometer. Cyclic Voltammetry (CV) and ECL measurements were carried out by ECL analysis system for multi-detector and Electrochemical Analyzer (Xi'anruimai Analytical Instruments Co., Ltd.) at room temperature.

4.2. Materials and reagents

The cyclometalated ligands 2-(4-fluorophenyl)-4-phenylpyridine (FPP), 1-(4-fluorobenzyl)-2-(4-fluorophenyl)-1H-benzo[d]imidazole (FBPI) and 2,5-dip-tolyl-1, 3,4-oxadiazole (MDX) were made according to the literature procedure [28,29]. $\text{IrCl}_3 \cdot 3\text{H}_2\text{O}$ $\text{Ru}(\text{bpy})_3\text{Cl}_2 \cdot 6\text{H}_2\text{O}$ (98%), Tetra-n-butylammonium hexafluorophosphate (Bu_4NPF_6), tri-n-propylamine (TPA) and Triton X-100 were purchased from Aldrich and used without further purification. Potassium phosphate buffer solutions were prepared with deionized water. Buffer Solutions containing TPA were prepared similarly except that it was necessary to stir vigorously to completely dissolve the amine. Other chemicals and solvents were all of reagent grade for synthesis and used as received.

4.3. Synthesis of iridium(III) complexes

Iridium(III) complexes $\text{Ir}(\text{FPP})_2(\text{acac})$, $\text{Ir}(\text{FBPI})_2(\text{acac})$, $\text{Ir}(\text{FBPI})_2(\text{pic})$, $\text{Ir}(\text{FBPI})_2(\text{pmp})$ and $\text{Ir}(\text{MDX})_2(\text{acac})$ were synthesized according to the literature procedure [31]. The mixture of cyclometalated ligand (FPP or FBPI, 2.2 mmol), $\text{IrCl}_3 \cdot 3\text{H}_2\text{O}$ (0.34 g, 1 mmol) in a mixed solvent of 2-ethoxyethanol (10 mL) and water (3 mL) was stirred under N_2 at 120 $^\circ\text{C}$ for 24 h. Cooled to room temperature, the precipitate was collected by filtration and washed with water, ethanol and acetone successively, and then dried in vacuum to give a cyclometalated Ir(III)-chloro-bridged dimer. The dimer (0.12 g, 0.08 mmol), the desired ancillary ligand (acetylacetonone, pmp or pic,

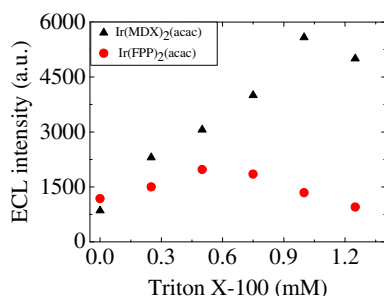


Fig. 6. ECL intensity vs concentration of surfactant for 10 μM $\text{Ir}(\text{FPP})_2(\text{acac})$ and $\text{Ir}(\text{MDX})_2(\text{acac})$ ($\text{CH}_3\text{CN}/\text{H}_2\text{O}$ (50:50, v/v)). Each point is the average of three scans.

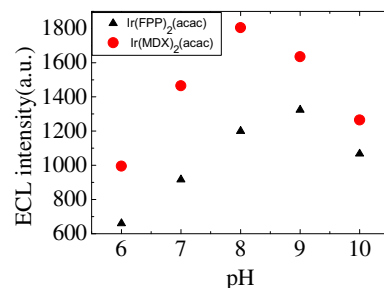


Fig. 7. ECL intensity vs pH for 10 μM $\text{Ir}(\text{FPP})_2(\text{acac})$ and $\text{Ir}(\text{MDX})_2(\text{acac})$ ($\text{CH}_3\text{CN}/\text{H}_2\text{O}$ (50:50, v/v)). Each point is the average of three scans.

0.24 mmol) and Na_2CO_3 (86 mg, 0.8 mmol) were dissolved in 2-ethoxyethanol (8 mL) and the mixture was then stirred under N_2 at 100 $^\circ\text{C}$ for 16 h. After cooling to room temperature, the precipitate was filtered and washed with water, ethanol and acetone. The crude product was flash chromatographed on silica gel using CH_2Cl_2 as eluent to afford the desired Ir(III) complex.

$\text{Ir}(\text{FPP})_2(\text{acac})$, Yield: 32%. ^1H NMR (CDCl_3 , 300 MHz) δ : 8.50 (d, $J = 6.0$ Hz, 2H), 8.00 (s, 2H), 7.80 (d, $J = 6.9$ Hz, 4H), 7.52–7.68 (m, 8H), 7.39 (d, $J = 6.0$ Hz, 2H), 6.58 (t, $J = 8.8$ Hz, 2H), 6.02 (d, $J = 9.8$ Hz, 2H), 5.29 (s, 1H), 1.86 (s, 6H). MS-ESI m/z : 787.8 (M^+). Elem anal. Calcd. for $\text{C}_{39}\text{H}_{29}\text{F}_2\text{N}_2\text{O}_2\text{Ir}$: C, 59.45; H, 3.71; N, 3.56. Found: C, 59.12; H, 3.83; N, 3.42. IR (KBr, cm^{-1}): 3443 (m), 2360 (m), 1614 (m), 1579 (s), 1533 (m), 1409 (s), 1185 (m), 868 (w), 762 (m), 669 (w).

$\text{Ir}(\text{FBPI})_2(\text{acac})$, Yield: 28%. ^1H NMR (CDCl_3 , 300 MHz) δ : 7.72 (d, $J = 7.6$ Hz, 2H), 7.29–7.38 (m, 6H), 7.15 (s, 2H), 7.01–7.06 (m, 8H), 6.34–6.37 (m, 2H), 6.05 (d, $J = 9.0$ Hz, 2H), 5.68–5.86 (m, 4H), 5.31 (s, 1H), 1.85 (s, 6H). MS-ESI m/z : 929.7 (M^+). Elem anal. Calcd. for $\text{C}_{45}\text{H}_{33}\text{N}_4\text{O}_2\text{F}_4\text{Ir}$: C, 58.12; H, 3.58; N, 6.02. Found: C, 58.15; H, 3.65; N, 6.13. IR (KBr, cm^{-1}): 3440 (w), 3055 (w), 1585 (s), 1512 (s), 1498 (m), 1417 (m), 1308 (m), 1257 (s), 1232 (s), 1068 (m), 847 (w), 820 (w), 757 (m).

$\text{Ir}(\text{FBPI})_2(\text{pic})$, Yield: 38%. ^1H NMR (CDCl_3 , 300 MHz) δ : 8.15 (d, $J = 7.6$ Hz, 2H), 7.73–7.87 (m, 6H), 7.26–7.33 (m, 2H), 7.12–7.20 (m, 8H), 6.72–6.75 (m, 2H), 6.14–6.16 (m, 4H), 5.50–5.75 (m, 4H). MS-ESI m/z : 938.9 (M^+). Elem anal. Calcd. for $\text{C}_{46}\text{H}_{30}\text{N}_4\text{F}_4\text{O}_2\text{Ir}$: C, 58.84; H, 3.22; N, 5.97. Found: C, 58.75; H, 3.15, N, 6.03. IR (KBr, cm^{-1}): 3448 (w), 3065 (w), 1659 (s), 1637 (m), 1599 (s), 1562 (m), 1510 (s), 1461 (m), 1432 (m), 1351 (m), 1332 (m), 1279 (m), 1254 (m), 1233 (m), 1192 (m), 1164 (m), 1100 (w), 816 (m), 758 (m), 746 (m), 693 (w).

$\text{Ir}(\text{FBPI})_2(\text{pmp})$, Yield: 35%. ^1H NMR (CDCl_3 , 300 MHz) δ : 8.07 (d, $J = 7.9$ Hz, 1H), 7.86 (d, $J = 7.6$ Hz, 1H), 7.41–7.44 (m, 2H), 7.32–7.36 (m, 4H), 7.21–7.23 (m, 2H), 7.14–7.16 (m, 3H), 7.02–7.07 (m, 7H), 6.87–6.89 (m, 3H), 6.23–6.38 (m, 5H), 6.00–6.07 (m, 2H), 5.99 (s, 2H), 5.53–5.64 (m, 4H). MS-ESI m/z : 1027.0 (M^+). Elem anal. Calcd. for $\text{C}_{53}\text{H}_{36}\text{N}_5\text{F}_4\text{OIr}$: C, 61.98; H, 3.53; N, 6.82. Found: C, 62.03; H, 3.55; N, 6.73. IR (KBr, cm^{-1}): 3447 (m), 2924 (w), 2344 (w), 16079 (s), 1561 (m), 1510 (m), 1463 (m), 1433 (m), 1354 (w), 1279 (w), 1254 (w), 1230 (w), 1190 (m), 1168 (w), 1125 (w), 825 (w), 697 (w).

$\text{Ir}(\text{MDX})_2(\text{acac})$, Yield: 32%. ^1H NMR (CDCl_3 , 300 MHz) δ : 8.15 (d, $J = 8.2$ Hz, 4H), 7.51 (d, $J = 7.6$ Hz, 2H), 7.41 (d, $J = 8.2$ Hz, 4H), 6.75 (d, $J = 7.6$ Hz, 2H), 6.54 (s, 2H), 5.30 (s, 1H), 2.49 (s, 6H), 2.18 (s, 6H), 1.92 (s, 6H). MS-ESI m/z : 789.8 (M^+). Elem anal. Calcd. for $\text{C}_{37}\text{H}_{33}\text{N}_4\text{O}_4\text{Ir}$: C, 56.25; H, 4.21; N, 7.09. Found: C, 56.13; H, 4.13; N, 7.18. IR (KBr, cm^{-1}): 3445 (m), 2918 (w), 1584 (s), 1514 (s), 1498 (m), 1449 (m), 1403 (m), 1256 (m), 1149 (w), 1040 (w), 985 (w), 821 (w), 749 (w), 722 (w).

4.4. X-ray crystallography

Suitable crystals of $\text{Ir}(\text{FPP})_2(\text{acac})$ and $\text{Ir}(\text{MDX})_2(\text{acac})$ were obtained by slow evaporation of isobutanol into an CH_2Cl_2 solution

of iridium complexes at room temperature. Diffraction data for compound Ir(FPP)₂(acac) and Ir(MDX)₂(acac) were collected at $T = 298(2)$ K. The data set was collected on a Bruker SMART APEX CCD diffractometer with graphite monochromated Mo K α radiation ($\lambda = 0.71073$ Å). The cell parameters for the iridium complexes were obtained from a least-squares refinement of the spots (from 60 collected frames) using the SMART program [32]. All of the calculations for the structure determination were carried out using the SHELXTL package (version 5.1) [33]. Initial atomic positions were located by Patterson methods using XS, and the structure of Ir(FPP)₂(acac) was refined by least-squares methods using SHELXTL package (version 5.1) with 3131 independent reflections within the range of $\theta = 2.0$ – 26.0° . The data for Ir(MDX)₂(acac) were $\theta = 2.1$ – 26.0° . Absorption corrections were applied by using SADABS [34]. Calculated hydrogen positions were input and refined in a riding manner along with the attached carbons.

4.5. Absorption, emission spectroscopy and ECL measurement

The absorbance and luminescence spectra of the complexes were obtained in CH₃CN solutions. PL detection was performed in the range of 450–700 nm. The relative luminescence efficiency was measured using an optically diluted CH₃CN solution ($OD < 0.05$ at the excitation wavelength) and calibrated with Ru(bpy)₃²⁺ in H₂O ($\Phi_{em} = 0.042$) as a standard according to the procedure reported elsewhere [35].

The ECL measurements were carried out in CH₃CN, mixed CH₃CN/H₂O (50:50, v/v), respectively, with TPA as an oxidative–reductive co-reactant. Tetrabutylammonium hexafluorophosphate (Bu₄NPF₆) was used as supporting electrolyte for CH₃CN solution. Buffer solutions were prepared with deionized water that had been passed through a Barnsted/Thermolyne filtration system.

The electrochemical and ECL experiments were carried out using a three-electrode system consisting of Ag/AgCl gel electrode (0.20 V vs NHE) (aqueous and mixed solvent) or Ag/Ag⁺ (0.01 M AgNO₃ in CH₃CN) as reference electrode (non-aqueous solvent), a platinum wire as counter electrode and a 2 mm-diameter platinum disk as working electrode. The working electrode was polished on a felt with 0.05 mm alumina, sonicated and rinsed with deionized water prior to each experiment. All electrochemical potentials were calibrated against Fc/Fc⁺ by the addition of ferrocene as an internal standard. All of the $E_{1/2}$ potentials have been directly obtained from cyclic voltammetric (CV) curves as averages of the cathodic and anodic peak potentials.

ECL efficiencies (Φ_{ecl}) were obtained by the literature methods [12,36], using Ru(bpy)₃²⁺ ($\Phi_{ecl} = 1$) as the standard. Reported values are the average of at least three scans with a relative standard deviation of $\pm 5\%$ for CH₃CN and CH₃CN/H₂O (50:50 v/v).

Acknowledgment

This work was financially supported by the Natural Science Foundation of China (No. 21075073 and No. 20971076).

Appendix A. Supplementary data

CCDC 791530 and 791531 contain the supplementary crystallographic data for this paper. These data can be obtained free of charge from the Cambridge Crystallographic Data Centre via www.ccdc.cam.ac.uk/data_request/cif.

References

- [1] M.M. Richter, Chem. Rev. 104 (2004) 3003–3036.
- [2] W.J. Miao, Chem. Rev. 108 (2008) 2506–2553.
- [3] H. Wei, E. Wang, Trends Anal. Chem. 27 (5) (2008) 447–459.
- [4] X.-B. Yin, S. Dong, E. Wang, Trends Anal. Chem. 23 (6) (2004) 432–441.
- [5] A.W. Knight, G.M. Greenway, Analyst 119 (1994) 879–890.
- [6] W.-Y. Lee, Mikrochim. Acta 127 (1997) 19–39.
- [7] N.R. Armstrong, M. Wightman, E.M. Gross, Annu. Rev. Phys. Chem. 52 (2001) 391–422.
- [8] E.M. Gross, J.D. Anderson, A.F. Slaterbeck, S. Thayumanavan, S. Barlow, Y. Zhang, S.R. Marder, H.K. Hall, M.F. Nabor, J.-F. Wang, E.A. Mash, N.R. Armstrong, R.M. Wightman, J. Am. Chem. Soc. 122 (2000) 4972–4979.
- [9] E.M. Gross, N.R. Armstrong, R.M. Wightman, J. Electrochem. Soc. 149 (2002) E137–E142.
- [10] H.D. Abruna, J. Electroanal. Chem. 175 (1984) 321–325.
- [11] M.M. Richter, A.J. Bard, Anal. Chem. 68 (1996) 2641–2650.
- [12] C.X. Li, G.H. Zhang, H.-H. Shih, X.Q. Jiang, P.P. Sun, Y. Pan, C.-H. Cheng, J. Organomet. Chem. 694 (2009) 2415–2420.
- [13] D. Bruce, M.M. Richter, Anal. Chem. 74 (2002) 1340–1342.
- [14] C. Cole, B.D. Muegge, M.M. Richter, Anal. Chem. 75 (2003) 601–604.
- [15] B.D. Muegge, M.M. Richter, Luminescence 20 (2005) 76–80.
- [16] B. Marco, B. Michele, V. Giovanni, P. Fabio, M. Magda, U.-R. Achille, M. Massimo, Inorg. Chem. 49 (2010) 1439–1448.
- [17] J.I. Kim, I.-S. Shin, H. Kim, J.-K. Lee, J. Am. Chem. Soc. 127 (2005) 1614–1615.
- [18] A. Kapturkiewicz, G. Angulo, Dalton Trans. (2003) 3907–3913.
- [19] B.D. Muegge, M.M. Richter, Anal. Chem. 76 (2004) 73–77.
- [20] J.B. Waern, C. Desmaretts, L.-M. Chamoreau, H. Amouri, A. Barbieri, Inorg. Chem. 47 (2008) 3340–3348.
- [21] T. Sajoto, P.I. Djurovich, A. Tamayo, M. Yousufuddin, R. Bau, M.E. Thompson, Inorg. Chem. 44 (2005) 7992–8003.
- [22] I.-S. Shin, J.I. Kim, T.-H. Kwon, J.-I. Hong, J.-K. Lee, H. Kim, J. Phys. Chem. C 111 (2007) 2280–2286.
- [23] A. Kapturkiewicz, J. Nowackib, P. Borowicza, Electrochimica Acta 50 (2005) 3395–3400.
- [24] M.-G. Colombo, T.-C. Brunold, T. Riedner, H.U. Güudel, M. Förtsch, H.-B. Bürgi, Inorg. Chem. 33 (1994) 545–551.
- [25] P.J. Hay, J. Phys. Chem. A 106 (2002) 1634–1641.
- [26] M. Bandini, M. Bianchi, G. Valenti, et al., Inorg. Chem. 49 (2010) 1439–1448.
- [27] C. Dragonetti, L. Falciola, P. Mussini, et al., Inorg. Chem. 46 (2007) 8533–8540.
- [28] S. Stagni, S. Collella, A. Palazzi, et al., Inorg. Chem. 47 (2008) 10509–10518.
- [29] M. Nonoyama, Bull. Chem. Soc. Jpn. 47 (1974) 767–770.
- [30] M.M. Richter, A.J. Bard, W.K. Kim, R.H. Schmehl, Anal. Chem. 70 (1998) 310–318.
- [31] J.V. Caspar, T.J. Meyer, J. Am. Chem. Soc. 105 (1983) 5583–5590.
- [32] Smart & SAINT Software Reference Manuals, Version 5.051. Bruker Analytical X-ray Instruments Inc, Madison, WI, 1998.
- [33] G.M. Sheldrick, SHELXTL Plus Structure Determination Package, Version 5.1. Bruker Analytical X-ray Instruments Inc, Madison, WI, 1998.
- [34] G.M. Sheldrick, SADABS, Program Empirical Absorption Correction. University of Göttingen, Göttingen, Germany, 1996.
- [35] H.S. White, A.J. Bard, J. Am. Chem. Soc. 104 (1982) 6891–6895.
- [36] P.P. Sun, C.M. Li, Y. Pan, Y. Tao, Synth. Metals 156 (2006) 525–528.